Two-loop mixed QCD-EW corrections to $q\overline{q} \to Hg$, $qg \to Hq$, and $\overline{q}g \to H\overline{q}$

Marco Bonetti,[a] **Erik Panzer**[b] **and Lorenzo Tancredi**[c]

[a]*Institute for Theoretical Particle Physics and Cosmology, RWTH Aachen University,*
Sommerfeldstrasse 16, D-52056 Aachen, Germany

[b]*Mathematical Institute, University of Oxford,*
OX2 6GG Oxford, U.K.

[c]*Physik Department, Technische Universität München,*
James-Franck-Straße 1, 85748 Garching, Germany

E-mail: bonetti@physik.rwth-aachen.de, erik.panzer@maths.ox.ac.uk,
lorenzo.tancredi@tum.de

ABSTRACT: We compute the two-loop mixed QCD-Electroweak corrections to $q\overline{q} \to Hg$ and its crossed channels $qg \to Hq$, $\overline{q}g \to H\overline{q}$, limiting ourselves to the contribution of light virtual quarks. We compute the independent helicity amplitudes as well as the form factors for this process, expressing them in terms of hyperlogarithms with algebraic arguments. The Feynman integrals are computed by direct integration over Feynman parameters and the results are expressed in terms of a basis of rational prefactors.

Contents

1 Introduction

The discovery of the Higgs boson at the CERN LHC in 2012 [1, 2] can be considered, beyond doubts, one of the greatest achievements of the high-energy physics program of the 21st century. This long anticipated particle crowns the Standard Model as a solid theory of reality and the study of its properties has the potential to help elucidate the mechanism of Electroweak (EW) symmetry breaking and to shed light on possible new physics scenarios beyond the Standard Model.

Since the Higgs discovery, the LHC has demonstrated not only to be a discovery machine, but also an impressive precision physics laboratory. In fact, in the past decade astonishing experimental results have been obtained by the LHC collaborations, which have made it possible to rediscover the Standard Model of particle physics and to perform cutting edge precision measurements, in some cases way beyond the original expectations. As the result of these impressive performances, the theoretical particle physics community has taken over the challenge of pushing theoretical predictions to similar degrees of precision. In particular, while the exact experimental precision achievable depends on the process considered, it has been shown that reaching the goal of the $\sim \mathcal{O}(1\%)$ level accuracy at the LHC for various important observables is within reach [3]. This will be possible not only because of the large statistics that will be accumulated at the LHC and its high luminosity upgrade (HL-LHC), but also thanks to refined techniques for the determination of interaction luminosity [4, 5] and for jet reconstruction [6, 7]. Among the observables that are most promising, a special role is played by the Higgs transverse momentum ($p_\perp$) distribution. The Higgs $p_\perp$ is

particularly interesting since a precision comparison of the measured distribution with similarly precise theoretical predictions could allow us, among other things, to obtain precious indirect information on the Higgs couplings and therefore on the details of the Spontaneous Symmetry Breaking (SSB) mechanism, see for example ref. [8].

The theoretical determination of the Higgs $p_\perp$ distribution at the LHC at the percent precision level involves the calculations of the production of a Higgs boson in addition to QCD radiation in hadron-hadron scattering $pp \to H + X$, which can be mediated at the elementary level by different types of interactions. As it is well known, due to the very high gluon luminosity, the main channel of production for the Higgs boson at the LHC is gluon fusion, in particular in those configurations where the Higgs boson couples to gluons through a loop of top quarks. This interaction process has been computed to Next-to-Next-to-Leading-Order (NNLO) in pure QCD retaining full dependence on the top-quark mass [9–13], while it is known up to N^{3}LO in QCD in the limit of infinite top-quark mass [14, 15]. This so-called Higgs Effective Field Theory (HEFT) has proven to be surprisingly reliable to describe higher-order QCD contributions. In fact, in this approximation, the N^{3}LO amounts to around 5% of the total cross section with a scale uncertainty of $\sim 2\%$ [16]. At this impressive level of precision, a proper treatment of sub-leading production modes and uncertainties becomes mandatory. Together with the absence of N^{3}LO parton distribution functions, the two other main sources of theoretical uncertainty are the impact of finite quark-mass effects and the NLO QCD corrections to the electroweak (EW) production modes [16], which usually go under the name of QCD-EW corrections and are the main focus of this paper.

As is the case in pure QCD, also QCD-EW corrections can affect different production channels. The most important one at the LHC is once again the gluon fusion channel. QCD-EW corrections to this production channel contribute in two different configurations: the first class of diagrams involves the effect of EW corrections to the standard ggH coupling through a massive top loop. This contribution has been shown to be extremely small already at LO, contributing to less than 1% to the total cross-section [17]. The second class of diagrams involves instead a loop of light quarks which connects the gluons to a pair of EW bosons, which then fuse to generate the Higgs. This production channel increases the total cross section at LO by around 5% with respect to the pure QCD corrections [12, 18–25] and, since NLO QCD corrections to Higgs production in gluon fusion can be as large as the LO contribution, a full account of these higher order corrections is essential to keep the theory uncertainty under control at the percent level. NLO QCD-EW effects in this channel have been estimated first in the unphysical limit $m_H \ll m_V$ with $V = W, Z$ in ref. [26], then by treating the real emissions in the soft-gluon approximation in refs. [27, 28] and more recently with full dependence on the Higgs and the vector boson masses and on the external QCD radiation in refs. [29–32].

In addition to the gluon-initiated diagrams, mixed QCD-EW corrections to $pp \to H + X$ also receive contributions from diagrams that involve a pair of quarks. There are in particular three relevant partonic channels, $qg \to Hq$, $\bar{q}g \to H\bar{q}$, and $q\bar{q} \to Hg$, which at LO proceed through a loop of virtual electroweak vector bosons. Their impact both at Tevatron and at the LHC was estimated for the first time in [33] for a Higgs mass of $m_H = 120\,\text{GeV}$. There it

was shown that, as expected, their relative weight at the LHC is smaller than at the Tevatron, due to the much larger gluon luminosity, but it is still sizable: in particular, the LO diagrams are responsible for a -3% shift in the $p_\perp$ distribution for values $100\,\text{GeV} \leq p_\perp \leq 300\,\text{GeV}$. With the goal of pushing theoretical uncertainties in Higgs distributions at the percent level, it is therefore important to consider also NLO corrections to this channel, first of all to obtain a reliable estimate of their uncertainty, and also to account for their possible non-trivial effects on the shape of the distributions.

One-loop mixed QCD-EW contributions containing light quarks as external states have been thoroughly investigated in [34], therefore the last missing building blocks are the relevant two-loop amplitudes. In this paper, we focus on their analytic calculation, liming ourselves to those contributions which involve only massless virtual quarks, similarly to what was done in [30]. Together with the phenomenological motivation, this calculation is interesting also from a formal point of view. Indeed, despite some similarities with the purely gluonic case described in [30], the quark induced channels are substantially more complicated for at least two reasons. First of all, they involve new classes of integrals that were entirely absent in the gluon induced ones. Moreover, at variance with the gluonic channel, these amplitudes have a non-trivial infrared structure and, for this reason, their finite remainders require a larger number of weight four functions. From a purely mathematical viewpoint, this calculation is particularly interesting due to the presence of a large number of square roots in the symbol of the relevant two-loop master integrals. In fact, while all integrals turn out to be linearly reducible [35, 36] and can therefore be expressed in terms of hyperlogarithms by direct integration over their Feynman-Schwinger parameter representation algorithmically [37], the presence of a large number of square roots renders the application of standard algorithms to handle and simplify the resulting expressions highly non-trivial.

The paper is organized as follows. In section 2 we discuss the structure of the amplitude, and in particular the treatment of vector and axial EW couplings; we then describe how to relate the helicity amplitudes to the two form factors composing the amplitude, and how to extract said form factors; at last, we give our convention for the integral families and integration measure. In section 3 we discuss the computational framework we used, first to evaluate the master integrals, and secondly to reduce the expressions to a minimal set of algebraic prefactors times a set of polylogarithmic functions. In section 4 we discuss the UV renormalization of the amplitude and the structure of IR divergences, extracting the finite remainder for the virtual corrections. We review our results and draw our conclusions in section 5.

We provide the list of master integrals for the LO and virtual NLO amplitude in appendix A. The analytic expressions of the finite remainders, as well as of the master integrals, are provided in the supplementary material attached to this paper.

2 The scattering amplitude

Our goal is to compute the two-loop mixed QCD-EW corrections to the three partonic scattering processes $qg \to Hq$, $\bar{q}g \to H\bar{q}$, and $q\bar{q} \to Hg$. To do so, we start by considering the decay of a Higgs boson to a quark-antiquark pair and a gluon

$$H(\mathbf{p}_4) \to q(\mathbf{p}_1) + \bar{q}(\mathbf{p}_2) + g(\mathbf{p}_3), \tag{2.1}$$
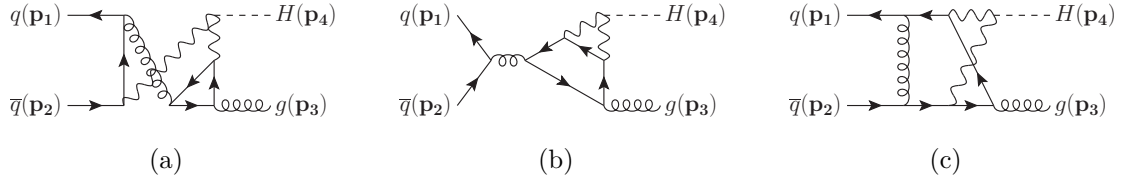
Figure 1. Representative diagrams for the process $H \to q\bar{q}g$. The internal wavy lines represent massive vector bosons. All momenta are taken to be incoming.

where the Higgs boson couples to the quarks through a pair of massive vector bosons V, where V is either equal to $W^{\pm}$ or Z, see figure 1.

The scattering amplitude for this process, $\mathcal{M}$, depends on the three Mandelstam variables

$$s = (p_1 + p_2)^2, \quad t = (p_1 + p_3)^2, \quad u = (p_2 + p_3)^2, \quad \text{with} \quad s + t + u = m_h^2, \quad (2.2)$$

and on the mass of the vector boson that mediates the interaction between the Higgs boson and the massless quarks, denoted as m_V. Throughout, m_h indicates the Higgs boson mass. The dependence of the scattering amplitude on the SU(3) color structure is given by the Gell-Mann matrices $T_{i_1 i_2}^{c_3}$, where c_3 is the color index associated with the gluon, and i_1 (i_2) is the color index of the quark (antiquark)

$$
\begin{aligned}
\mathcal{M}_{s_1 s_2 \lambda_3}(\mathbf{p}_1, \mathbf{p}_2, \mathbf{p}_3) &= \left[\frac{\alpha^{3/2} m_W}{2 \sin^3 \theta_W} \right] T_{i_1 i_2}^{c_3} A_{s_1 s_2 \lambda_3}(\mathbf{p}_1, \mathbf{p}_2, \mathbf{p}_3) \\
&= \left[\frac{\alpha^{3/2} m_W}{2 \sin^3 \theta_W} \right] T_{i_1 i_2}^{c_3} \epsilon_{\lambda_3}^{*\mu}(\mathbf{p}_3) \overline{u}_{s_1}(\mathbf{p}_1) \mathcal{A}_\mu(s, t, u, m_V^2) v_{s_2}(\mathbf{p}_2).
\end{aligned}
\quad (2.3)
$$

In eq. (2.3) we have collected out the overall electroweak coupling and we also made explicit the dependence on the spin of the quarks (s_1, s_2) and on the polarization vector of the gluon ϵ_{λ_3} which satisfies $\epsilon_{\lambda_3} \cdot p_3 = 0$. In addition, Ward Identities require that the amplitude $\mathcal{A}_\mu(s, t, u, m_V^2)$ must satisfies the transversality condition

$$p_3 \cdot \mathcal{A}(s, t, u, m_V^2) = 0. \quad (2.4)$$

We write the coupling of the vector boson V with the light quarks as $g_V^v + \gamma_5 g_V^a$, where [38]

$$
\begin{aligned}
g_W^v &= -\mathrm{i} \frac{e}{\sin \theta_W} \frac{1}{2\sqrt{2}}, & g_W^a &= +\mathrm{i} \frac{e}{\sin \theta_W} \frac{1}{2\sqrt{2}}, \\
g_{Zf}^v &= -\mathrm{i} \frac{e}{\sin \theta_W \cos \theta_W} \left[\frac{T_f}{2} - Q_f \sin^2 \theta_W \right], & g_{Zf}^a &= -\mathrm{i} \frac{e}{\sin \theta_W \cos \theta_W} \left[\frac{T_f}{2} \right].
\end{aligned}
\quad (2.5)
$$

Q_f and T_f are the electric charge and the eigenvalue of the third generator of SU(2)$_L$, both associated to the fermion f interacting with V, e is the absolute value of the electric charge of the electron, and θ_W is the weak mixing angle. In what follows we also define $e = \sqrt{4\pi\alpha}$ for the electroweak coupling and $g_S = \sqrt{4\pi\alpha_S}$ for the strong coupling.

It is useful to separate the amplitude into different contributions, depending on how the electroweak bosons are coupled to the rest of the diagram; clearly, depending on the number of loops we are interested in, different contributions can play a role. If we limit ourselves to consider Feynman diagrams up to order $\mathcal{O}(\alpha^{3/2}\alpha_S^{3/2})$, there are only two possible non-zero classes of diagrams that can contribute, which we call *open* and *closed*. In particular, we write

$$\mathcal{A}_\mu(\mathbf{p}_1, \mathbf{p}_2, \mathbf{p}_3) = \mathcal{A}_\mu^{\text{open}}(\mathbf{p}_1, \mathbf{p}_2, \mathbf{p}_3) + \mathcal{A}_\mu^{\text{closed}}(\mathbf{p}_1, \mathbf{p}_2, \mathbf{p}_3) \qquad (2.6)$$

where $\mathcal{A}_\mu^{\text{open}}$ receives contribution from those diagrams where the two vector bosons are both attached to the external fermion line, see figure 1(c), while $\mathcal{A}_\mu^{\text{closed}}$ encompasses the diagrams where both vector bosons couple to a closed fermion loop, see figure 1(b).

Let us start by considering $\mathcal{A}_\mu^{\text{open}}$. Feynman diagrams of this type start contributing at one-loop order. The EW bosons couple to the fermion line both through vector and axial terms (depending on the chirality of the external quarks) but it is possible to bypass the explicit manipulation of terms containing γ_5 by considering polarized external states: by anticommuting γ_5 until it touches the spinor $\overline{u}_{L/R}(\mathbf{p}_1)$, such a matrix coming from the EW vertices is absorbed into the left- or right-chirality projectors $\mathbb{P}_L = \frac{1-\gamma_5}{2}$ and $\mathbb{P}_R = \frac{1+\gamma_5}{2}$, respectively. The resulting expressions for the helicity amplitudes do not contain γ_5 anymore and can be computed assuming that the electroweak bosons only couple through a vector current to the fermion line, with an overall coupling coefficient determined by type and chirality of the quark $q(\mathbf{p}_1)$. Specifically, for $\overline{u}_L(\mathbf{p}_1) = \overline{u}(\mathbf{p}_1)\mathbb{P}_L$ we obtain

$$\mathcal{A}_{L,\mu}^{\text{open}} = \left(\frac{2}{\cos^4\theta_W} Q_q^2 \sin^4\theta_W \right) \mathbb{P}_L \left[\tau_{1,\mu} F_{1,m_Z}^{\text{open}} + \tau_{2,\mu} F_{2,m_Z}^{\text{open}} \right], \qquad (2.7)$$

where, as in eq. (2.5), Q_q is the electric charge of the quark $q(\mathbf{p}_1)$, and we define

$$F_{i,m_X} = F_i(s, t, u, m_h^2, m_V^2 = m_X^2), \qquad (2.8)$$

and

$$\tau_{1\mu} = \not{p}_3 p_{2\mu} - p_2 \cdot p_3 \gamma_\mu, \qquad\qquad \tau_{2,\mu} = \not{p}_3 p_{1\mu} - p_1 \cdot p_3 \gamma_\mu. \qquad (2.9)$$

For $\overline{u}_R(\mathbf{p}_1) = \overline{u}(\mathbf{p}_1)\mathbb{P}_R$ we get

$$\begin{aligned}
\mathcal{A}_{R,\mu}^{\text{open}} = \Bigg\{ & \mathbb{P}_R \left[\tau_{1,\mu} F_{1,m_W}^{\text{open}} + \tau_{2,\mu} F_{2,m_W}^{\text{open}} \right] \\
& + \frac{2}{\cos^4\theta_W} \left(T_q - Q_q \sin^2\theta_W \right)^2 \mathbb{P}_R \left[\tau_{1,\mu} F_{1,m_Z}^{\text{open}} + \tau_{2,\mu} F_{2,m_Z}^{\text{open}} \right] \Bigg\}.
\end{aligned} \qquad (2.10)$$

The different form of the couplings between eq. (2.7) and eq. (2.10) is due to the fact that $\mathcal{A}_{L,\mu}^{\text{open}}$ receives contributions from the Z boson only, while $\mathcal{A}_{R,\mu}^{\text{open}}$ is sensitive to the W boson as well. We assume the Cabibbo-Kobayashi-Maskawa mixing matrix to be the identity matrix.[1]

Starting at two loops, one can draw diagrams where either one or both EW bosons couple to an internal light-quark loop, see figures 1(a) and 1(b), respectively. For those diagrams where a single EW boson attaches to the fermion loop, it is possible to show that

---

[1]This approximation is justified because the off-diagonal entries are strongly suppressed.

both the vector and the axial contribution vanish at the level of the amplitude: the axial part cancels out adding together degenerate isospin doublets, while the vector contribution must add up to zero due to Furry's theorem. In case of both the EW vector bosons attached to the same light-quark loop, two contributions are possible: one proportional to $(g_V^v)^2 + (g_V^a)^2$ and independent from γ_5, and one proportional to $g_V^v g_V^a \gamma_5$. This last contribution vanishes identically when summing over degenerate isospin doublets. This clearly does not apply to the third quark doublet. In diagrams containing $W^\pm$ bosons we avoid the issue by not allowing top and bottom quarks circulating in the internal loop, while we consider all but the top quark in loops coupled with Z bosons, since we expect that the missing axial contributions will be suppressed.

We collect the contribution of the diagrams containing a closed quark loop to the amplitude $\mathcal{A}_\mu$ under the label $\mathcal{A}_\mu^{\text{closed}}$. As explained above, up to their contribution to the overall coupling factor, the amplitude contains no axial terms and it can be decomposed in form factors following the same procedure as for the amplitude $H \to q\bar{q}g$ in pure QCD, see [39]. It reads

$$
\mathcal{A}_\mu^{\text{closed}} = \frac{1}{2} \left\{ 4 \left[\tau_{1,\mu} F_{1,m_W}^{\text{closed}} + \tau_{2,\mu} F_{2,m_W}^{\text{closed}} \right] \right.
$$
$$
\left. + \frac{2}{\cos^4 \theta_W} \left(\frac{5}{4} - \frac{7}{3} \sin^2 \theta_W + \frac{22}{9} \sin^4 \theta_W \right) \left[\tau_{1,\mu} F_{1,m_Z}^{\text{closed}} + \tau_{2,\mu} F_{2,m_Z}^{\text{closed}} \right] \right\}, \tag{2.11}
$$

where the factor of 4 in the first line comes from diagrams containing the W boson (summed over the first two generations of quarks), while the term in round brackets in the second line stems from diagrams featuring the Z boson (summing on all quarks except the top). We stress also that, since the contribution $\mathcal{A}_\mu^{\text{closed}}$ only starts at the two-loop order, we have collected out one more factor of $\alpha_S^{1/2}$, compared to $\mathcal{A}_\mu^{\text{open}}$.

The form factors F_{j,m_V}^{open} and $F_{j,m_V}^{\text{closed}}$ that contribute to eqs. (2.7), (2.10), and (2.11) admit an expansion in the strong coupling constant

$$
F_{j,m_V}^{\text{open}} = \sqrt{\alpha_S} \left[F_{j,m_V}^{\text{open},(1)} + \left(\frac{\alpha_S}{2\pi} \right) F_{j,m_V}^{\text{open},(2)} + \mathcal{O}\left(\alpha_S^2 \right) \right],
$$
$$
F_{j,m_V}^{\text{closed}} = \sqrt{\alpha_S} \left[\left(\frac{\alpha_S}{2\pi} \right) F_{j,m_V}^{\text{closed},(2)} + \mathcal{O}\left(\alpha_S^2 \right) \right], \tag{2.12}
$$

where $F_{j,m_V}^{\text{class},(l)}$ is the l-loop contribution of the corresponding class of diagrams and, as always, m_V can be either m_Z or m_W. Finally, while $F_{j,m_V}^{\text{open},(1)}$ and $F_{j,m_V}^{\text{closed},(2)}$ have a trivial color structure, $F_{j,m_V}^{\text{open},(2)}$ can be decomposed as

$$
F_{j,m_V}^{\text{open},(2)} = N_c F_{j,m_V}^{N_c} + \frac{1}{N_c} F_{j,m_V}^{1/N_c}, \tag{2.13}
$$

where N_c is the number of colors.

2.1 Helicity amplitudes

When dealing with scattering amplitudes containing massless external states, helicity amplitudes are often the simplest physical objects to compute. We fix the helicities of

the external quark-antiquark pair and of the external gluons by use of the spinor-helicity formalism

$$\mathbb{P}_R u(\mathbf{p}) = u_R(\mathbf{p}) = v_R(\mathbf{p}) = |p\rangle, \qquad \mathbb{P}_L u(\mathbf{p}) = u_L(\mathbf{p}) = v_L(\mathbf{p}) = |p],$$
$$\overline{u}(\mathbf{p})\mathbb{P}_L = \overline{u}_L(\mathbf{p}) = \overline{v}_L(\mathbf{p}) = [p|, \qquad \overline{u}(\mathbf{p})\mathbb{P}_R = \overline{u}_R(\mathbf{p}) = \overline{v}_R(\mathbf{p}) = \langle p|,$$
$$\epsilon_+^{*\mu}(\mathbf{p_3}) = +\frac{\langle q\gamma^\mu 3]}{\sqrt{2}\langle q3\rangle}, \qquad \epsilon_-^{*\mu}(\mathbf{p_3}) = -\frac{[q\gamma^\mu 3\rangle}{\sqrt{2}[q3]}, \tag{2.14}$$

where q is a generic light-like vector that represents the gauge freedom associated to the external gluon. As in eq. (2.3), we indicate the helicity amplitudes as $A_{s_1 s_2 \lambda_3}$, where s_1, s_2 are the spins of the quarks while λ_3 is the polarisation of the gluon. There are two independent helicity amplitudes, which we choose to be A_{RL+} and A_{LR+}, while all other helicity configurations can be obtained from these two by parity and charge conjugation transformations, as exemplified below.

In the same way as we did for the full amplitude $\mathcal{A}_\mu$, we divide the helicity amplitude for $H \to q\overline{q}g$ into two separately gauge-invariant contributions

$$A_{s_1 s_2 \lambda_3} = A_{s_1 s_2 \lambda_3}^{\text{open}} + A_{s_1 s_2 \lambda_3}^{\text{closed}}. \tag{2.15}$$

By explicitly fixing the helicities of the external particles and keeping track of the electroweak couplings we find for the two different contributions

$$A_{RL+}^{\text{open}} = \left[F_{1,m_W}^{\text{open}} + \frac{2}{\cos^4\theta_W} \left(T_q - Q_q \sin^2\theta_W \right)^2 F_{1,m_Z}^{\text{open}} \right] \frac{s}{\sqrt{2}} \frac{[23]^2}{[12]}, \tag{2.16}$$

$$A_{LR+}^{\text{open}} = \left[\frac{2}{\cos^4\theta_W} Q_q^2 \sin^4\theta_W F_{2,m_Z}^{\text{open}} \right] \frac{s}{\sqrt{2}} \frac{[13]^2}{[12]}, \tag{2.17}$$

and

$$A_{RL+}^{\text{closed}} = \frac{1}{2} \left[4F_{1,m_W}^{\text{closed}} + \frac{2}{\cos^4\theta_W} \left(\frac{5}{4} - \frac{7}{3}\sin^2\theta_W + \frac{22}{9}\sin^4\theta_W \right) F_{1,m_Z}^{\text{closed}} \right] \frac{s}{\sqrt{2}} \frac{[23]^2}{[12]}, \tag{2.18}$$

$$A_{LR+}^{\text{closed}} = \frac{1}{2} \left[4F_{2,m_W}^{\text{closed}} + \frac{2}{\cos^4\theta_W} \left(\frac{5}{4} - \frac{7}{3}\sin^2\theta_W + \frac{22}{9}\sin^4\theta_W \right) F_{2,m_Z}^{\text{closed}} \right] \frac{s}{\sqrt{2}} \frac{[13]^2}{[12]}. \tag{2.19}$$

We stress that for $A_{s_1 s_2 \lambda_3}^{\text{open}}$ special care has to be taken to derive these formulas, taking into account the parity violating coupling of the EW bosons to the external quark line.

The remaining non-zero helicity amplitudes can be obtained by parity and charge conjugation transformations. For the *closed* contributions we get

$$A_{RL-}^{\text{closed}}(s, t, u, m_V^2) = \left(A_{LR+}^{\text{closed}}(s, t, u, m_V^2) \right)^*, \tag{2.20}$$

$$A_{LR-}^{\text{closed}}(s, t, u, m_V^2) = \left(A_{RL+}^{\text{closed}}(s, t, u, m_V^2) \right)^*, \tag{2.21}$$

where complex conjugation here is intended to act only on the spinor products: $[ij]^* = \langle ji\rangle$ and $\langle ij\rangle^* = [ji]$.

The *open* contributions require a bit more care to be obtained, and explicitly read

$$A_{RL-}^{\text{open}} = \left[F_{2,m_W}^{\text{open}} + \frac{2}{\cos^4 \theta_W} \left(T_q - Q_q \sin^2 \theta_W \right)^2 F_{2,m_Z}^{\text{open}} \right] \frac{s}{\sqrt{2}} \frac{\langle 13 \rangle^2}{\langle 12 \rangle} , \qquad (2.22)$$

$$A_{LR-}^{\text{open}} = \left[\frac{2}{\cos^4 \theta_W} Q_q^2 \sin^4 \theta_W F_{1,m_Z}^{\text{open}} \right] \frac{s}{\sqrt{2}} \frac{\langle 23 \rangle^2}{\langle 12 \rangle} . \qquad (2.23)$$

It is important to notice that, from their very definition in eqs. (2.10) and (2.11), the two form factors F_1^{closed} and F_2^{closed} are not independent, and instead are mapped into each other by exchanging p_1 and p_2, namely

$$F_1^{\text{closed}}(s, t, u, m_V^2) = F_2^{\text{closed}}(s, u, t, m_V^2) , \qquad (2.24)$$

implying that

$$\begin{aligned} A_{RL+}^{\text{closed}}(s, t, u, m_V^2) &= A_{LR+}^{\text{closed}}(s, u, t, m_V^2) , \\ A_{RL-}^{\text{closed}}(s, t, u, m_V^2) &= A_{LR-}^{\text{closed}}(s, u, t, m_V^2) . \end{aligned} \qquad (2.25)$$

Similarly, we observe that

$$F_1^{\text{open}}(s, t, u, m_V^2) = F_2^{\text{open}}(s, u, t, m_V^2) , \qquad (2.26)$$

while an identity analogous to eq. (2.25) does not hold in this case due to the dependence of the EW coupling on the helicity of the external particles.

We checked our expressions for the helicity amplitudes at LO against the computer code `OpenLoops` [40], finding excellent agreement.

2.2 Form factor evaluation

Here we focus on the calculation of the two-loop corrections to the form factors described above, namely to F_{j,m_V}^{class} with $V = W^\pm, Z$, and for the two classes of open and closed diagrams. At the two-loop order, the form factors for a given type of EW boson V receive contribution from 45 different two-loop Feynman diagrams, see figure 1. We generate them with the program `qgraf` [41]. The form factors F_j^{class} can then be extracted by applying the projectors $\mathcal{P}_j$ to the Feynman diagrams that contribute to $A_{s_1 s_2 \lambda_3}^{\text{class}}$, eq. (2.3), such as

$$F_j^{\text{class}} = \sum_{s_1, s_2, \lambda_3} A_{s_1 s_2 \lambda_3}^{\text{class}}(\mathbf{p}_1, \mathbf{p}_2, \mathbf{p}_3) \mathcal{P}_{j, \lambda_3 s_2 s_1} , \qquad (2.27)$$

where

$$\mathcal{P}_{1, \lambda_3 s_2 s_1} = \epsilon_{\lambda_3}^\nu(\mathbf{p}_3) \frac{1}{2(D-3)st} \left[\frac{D-2}{t} T_{1, \nu s_2 s_1}^\dagger - \frac{D-4}{u} T_{2, \nu s_2 s_1}^\dagger \right] , \qquad (2.28)$$

$$\mathcal{P}_{2, \lambda_3 s_2 s_1} = \epsilon_{\lambda_3}^\nu(\mathbf{p}_3) \frac{1}{2(D-3)su} \left[\frac{D-2}{u} T_{2, \nu s_2 s_1}^\dagger - \frac{D-4}{t} T_{1, \nu s_2 s_1}^\dagger \right] , \qquad (2.29)$$

with $T_{i, \mu s_1 s_2} = \overline{u}_{s_1}(\mathbf{p}_1) \tau_{i, \mu} v_{s_2}(\mathbf{p}_2)$ and $\tau_{i, \mu}$ as defined in eq. (2.9).

Denominator	Integral family PL	Integral family NA	Integral family NB
D_1	k_1^2	k_1^2	k_1^2
D_2	$k_2^2 - m_V^2$	$(k_1 - k_2)^2$	$(k_1 - k_2)^2$
D_3	$(k_1 - k_2)^2$	$(k_1 - p_1)^2$	$(k_1 - p_1)^2$
D_4	$(k_1 - p_1)^2$	$(k_2 + p_3)^2 - m_V^2$	$(k_2 + p_3)^2 - m_V^2$
D_5	$(k_1 - p_1 - p_2)^2$	$(k_1 - p_1 - p_2)^2$	$(k_1 - p_1 - p_2)^2$
D_6	$(k_1 - p_1 - p_2 - p_3)^2$	$(k_2 - p_1 - p_2)^2 - m_V^2$	$(k_2 - p_1 - p_2)^2 - m_V^2$
D_7	$(k_2 - p_1 - p_2 - p_3)^2 - m_V^2$	$(k_1 - k_2 - p_3)^2$	$(k_1 - k_2 - p_3)^2$
D_8	$(k_2 - p_1)^2$	$(k_2 - p_1)^2 - m_V^2$	$(k_2 - p_1)^2$
D_9	$(k_2 - p_1 - p_2)^2$	$(k_1 - p_1 - p_3)^2$	$(k_1 - p_1 - p_3)^2$

Table 1. Definition of the planar (PL) and non-planar (NA and NB) integral families. The loop momenta are denoted by k_1 and k_2, while m_V indicates the mass of the vector boson. The prescription $+i\epsilon$ is understood for each propagator and not written explicitly.

We use FORM [42, 43] to apply the projectors on the individual Feynman diagrams, carry out the Dirac algebra and express the form factors as linear combinations of scalar two-loop Feynman integrals. To describe all the integrals appearing in the amplitude we use three different integral families: one for planar integrals and two for non-planar integrals. We define such families as follows:
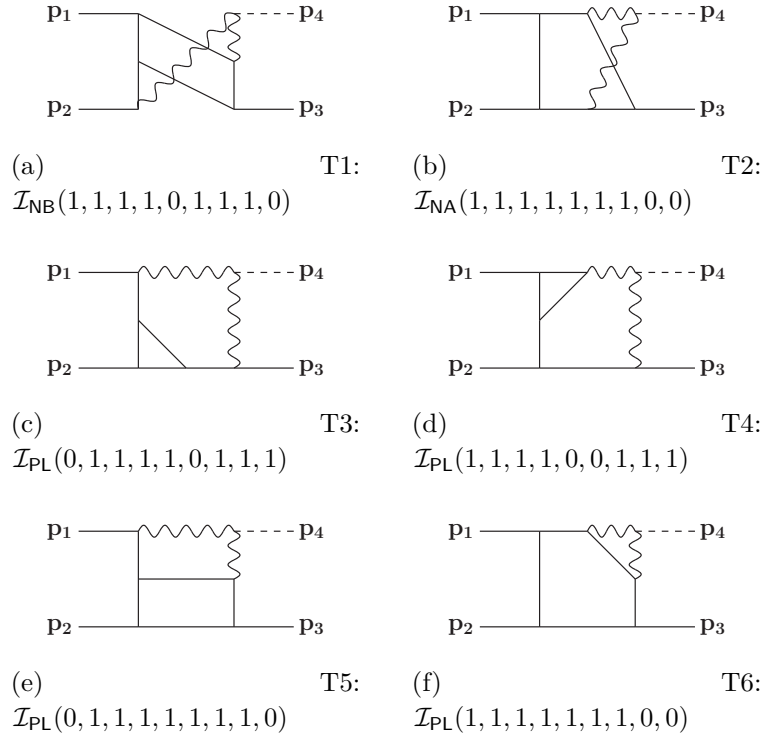
$$\mathcal{I}_{\text{top}}(a_1, a_2, \ldots, a_8, a_9) = \int \frac{\mathfrak{D}^d k_1 \, \mathfrak{D}^d k_2}{D_1^{a_1} D_2^{a_2} D_3^{a_3} D_4^{a_4} D_5^{a_5} D_6^{a_6} D_7^{a_7} D_8^{a_8} D_9^{a_9}} \,, \tag{2.30}$$

where $\text{top} \in \{\text{PL}, \text{NA}, \text{NB}\}$ labels the families and the denominators $D_1, \ldots, D_9$ are given in table 1. We use dimensional regularization with $d = 4 - 2\varepsilon$, and our convention for the integration measure for each loop is

$$\mathfrak{D}^d k = \frac{\mathrm{d}^d k}{i\pi^{d/2}\Gamma(1 + \varepsilon)} \,. \tag{2.31}$$

With the definitions given in table 1, the top sectors of each integral family appearing in the amplitude are depicted in figure 2. All the other diagrams contributing to the process can be obtained by permuting the external legs or by pinching the internal propagators.

We reduce the set of scalar integrals appearing in the amplitude to a basis of master integrals ([44–46]) by first using Reduze2 [47, 48] to map the Feynman diagrams to the relevant integral families and then performing the reduction to master integrals with KIRA [49]. We find that the independent helicity amplitudes can be written in terms of 69 master integrals (modulus permutations of the external legs), see appendix A for the full list. The master integrals obtained from the top sectors T_2 and T_6 have already been addressed in [30], while the remaining ones are new. We choose candidates for these new master integrals following the same prescriptions as for the $gg \to Hg$ case (for a detailed description, see [30]).

(a)   T1:
$\mathcal{I}_{\mathsf{NB}}(1,1,1,1,0,1,1,1,0)$

(b)   T2:
$\mathcal{I}_{\mathsf{NA}}(1,1,1,1,1,1,1,0,0)$

(c)   T3:
$\mathcal{I}_{\mathsf{PL}}(0,1,1,1,1,0,1,1,1)$

(d)   T4:
$\mathcal{I}_{\mathsf{PL}}(1,1,1,1,0,0,1,1,1)$

(e)   T5:
$\mathcal{I}_{\mathsf{PL}}(0,1,1,1,1,1,1,1,0)$

(f)   T6:
$\mathcal{I}_{\mathsf{PL}}(1,1,1,1,1,1,1,0,0)$

Figure 2. The six top sectors appearing in the amplitude. Straight (wavy) lines denote massless (massive) propagators. The dashed line indicates the Higgs boson. All momenta are taken to be incoming.

3 Computational details

The computation of the amplitude is in principle straightforward: by following the approach discussed in [30] for the $gg \to Hg$ amplitude, we compute the master integrals by direct integration over their Feynman-Schwinger parametrisation and we insert their expressions into the amplitude and collect common terms. However, in this case the size and complexity of both the expressions of the master integrals and the expressions of the form factors, together with the presence of UV and IR poles in ϵ, makes the computation highly non-trivial.

3.1 Evaluation of the master integrals

We write the integrals of each integral family in (2.30) as integrals over Feynman-Schwinger parameters x_i depending on the denominators D_i from table 1. In particular, the integrals are defined in terms of two polynomials $\mathcal{U}$ and $\mathcal{F}$ which are associated to each contributing top sector of the integral families considered [50].

Let us start considering the integrals associated to the top-sector T_3. In this case, the two polynomials read

$$\mathcal{U} = x_3(x_2 + x_4 + x_5 + x_7 + x_8 + x_9) + (x_4 + x_5)(x_2 + x_7 + x_8 + x_9) \tag{3.1}$$

$$\mathcal{F} = m_V^2(x_2 + x_7)\mathcal{U} - m_h^2 x_2 x_7(x_3 + x_4 + x_5),$$
$$- s x_2(x_3 x_5 + x_3 x_9 + x_4 x_9 + x_5 x_9) - u x_7(x_3 x_4 + x_3 x_8 + x_4 x_8 + x_5 x_8). \tag{3.2}$$

Applying the polynomial reduction algorithm [35, 36] as implemented in `HyperInt` [37], these polynomials are found to be linearly reducible. This means in particular that, for a suitable order of the Schwinger parameters x_i, the successive integrals over each x_i can be performed using `HyperInt`. For this particular case, it is easy to verify that we can integrate in the order $x_4, x_5, x_3, x_8, x_9, x_2$.[2] In turn, this means that all integrals associated to these two polynomials can then be expressed as linear combinations $\sum_k R_k G_k$ of hyperlogarithms G_k, which are iterated integrals

$$G\left(\sigma_1, \ldots, \sigma_n; z\right) = \begin{cases} (\log z)^n/n! & \text{if } \sigma_1 = \cdots = \sigma_n = 0 \text{ and} \\ \int_0^z \frac{\mathrm{d}t}{t-\sigma_1} G\left(\sigma_2, \ldots, \sigma_n; t\right) & \text{otherwise.} \end{cases} \quad (3.3)$$

These functions are often called *generalised harmonic polylogarithms* or *multiple polyloga-rithms* in the physics literature, see for example refs. [51–54]. Their arguments σ_i, z and coefficients R_k are algebraic functions of the variables s, t, u, m_V^2 (recall that $m_h^2 = s+t+u$ is not independent). More precisely, the polynomial reduction shows that σ_i, z, R_k are *rational* functions in s, t, u, m_V^2, r with the square root

$$r = m_h^2 \sqrt{1 - 4m_V^2/m_h^2}. \quad (3.4)$$

This root arises in the last integration (over x_2). The analysis of the planar top sector T_6 is very similar and discussed in detail in [30]. The conclusions are the same as for T_3.

The planar top sectors T_4 and T_5 are more complicated and introduce an additional square root in the final integration. This additional root is

$$\begin{aligned} r_{ust} &= \sqrt{s^2u^2 + 2su(t-s)m_V^2 + (s+t)^2m_V^4} &\text{for } T_4, \\ r_{sut} &= \sqrt{s^2u^2 + 2su(t-u)m_V^2 + (t+u)^2m_V^4} &\text{for } T_5. \end{aligned} \quad (3.5)$$

The Symanzik polynomials of the topology T_4 are

$$\mathcal{U} = x_3(x_1 + x_2 + x_4 + x_7 + x_8 + x_9) + (x_1 + x_4)(x_2 + x_7 + x_8 + x_9) \quad (3.6)$$

$$\begin{aligned} \mathcal{F} &= m_V^2(x_2 + x_7)\mathcal{U} - m_h^2 x_7(x_1x_2 + x_1x_3 + x_2x_3 + x_2x_4), \\ &- sx_9(x_1x_2 + x_1x_3 + x_2x_3 + x_2x_4) - ux_7(x_1x_8 + x_3x_4 + x_3x_8 + x_4x_8). \end{aligned} \quad (3.7)$$

These are linearly reducible and we can integrate e.g. in the order $x_1, x_4, x_3, x_8, x_9, x_2$ (setting $x_7 = 1$). The last integration over x_2 requires taking the roots r and r_{ust}, therefore any integral of the topology T_4 can be written with prefactors R_k and arguments of the hyperlogarithms G_k being rational functions of s, t, u, m_V^2, r, and r_{ust}.

The analysis of top sector T_5 is very similar. The conclusion is that all its integrals can be written in such a way that R_k and the arguments of G_k are rational in s, t, u, m_V^2, r, and r_{sut}.

The non-planar topology T_2 was already discussed in [30]. It produces prefactors R_k and arguments in the hyperlogarithms G_k that are rational functions of s, t, u, m_V^2 and four roots r, r_t, r_u, r_{tu}. We defined r above, and the additional roots are

$$r_t = \sqrt{r^2 - 4m_V^2 su/t}, \qquad r_u = \sqrt{r^2 - 4m_V^2 st/u}, \qquad r_{tu} = \sqrt{1 - 4m_V^2/(t+u)}. \quad (3.8)$$

---

[2] The last variable, x_7, is not integrated over, but set to $x_7 = 1$.

top sector	r	r_t	r_u	r_{tu}	r_{ust}	r_{sut}	r_{stu}	r_{uts}
T_1	•	•					•	•
T_2	•	•	•	•				
T_3	•							
T_4	•					•		
T_5	•						•	
T_6	•							

Table 2. The entries in this table indicate that a root appears in the prefactors or hyperlogarithm arguments of some Feynman integral of the sector.

Finally, also the non-planar topology T_1 turns out to be linearly reducible. The Symanzik polynomials are

$$\mathcal{U} = (x_1 + x_3)(x_2 + x_7) + (x_1 + x_2 + x_3 + x_7)(x_4 + x_6 + x_8) , \tag{3.9}$$

$$\mathcal{F} = m_V^2(x_4 + x_6)\mathcal{U} - m_h^2 x_6(x_1 x_4 + x_1 x_7 + x_2 x_4 + x_3 x_4 + x_4 x_7) - s x_1 x_2 x_6$$
$$- u x_3 x_6 x_7 - t(x_1 x_8(x_4 + x_7) + x_2 x_4(x_3 + x_8) + x_4 x_8(x_3 + x_7)) , \tag{3.10}$$

and $x_1, x_3, x_2, x_7, x_8, x_4$ is a linearly reducible integration order (setting $x_6 = 1$). The last integration (over x_4) introduces two additional square roots

$$r_{stu} = \sqrt{s^2 t^2 + 2st(u - t)m_V^2 + (t + u)^2 m_V^4} , \tag{3.11}$$

$$r_{uts} = \sqrt{u^2 t^2 + 2ut(s - t)m_V^2 + (s + t)^2 m_V^4} , \tag{3.12}$$

and, as a consequence, the integrals from topology T_1 will be expressed such that the prefactors R_k and arguments of the hyperlogarithms G_k are rational functions of $s, t, u, m_V^2, r, r_t, r_{stu}, r_{uts}$.

To summarize: all six top sectors are linearly reducible and hence the ϵ-expansion of all corresponding Feynman integrals can in principle be computed by integration over Schwinger parameters using hyperlogarithms. The resulting expressions are linear combinations of hyperlogarithms, with arguments and prefactors that are rational functions of s, t, u, m_V^2 and a number of square roots as indicated in table 2.

Since master integrals with external legs crossed are also required in the computation of the form factors, additional roots appear, all obtained from permuting s, t, and u in the definitions above. In particular, our results presented in the next section involve, in addition to the above, also the root

$$r_{tus} = \sqrt{t^2 u^2 + 2tu(s - u)m_V^2 + (s + u)^2 m_V^4}. \tag{3.13}$$

3.2 Construction of the form factors

The analytic expressions of the master integrals expanded in $\epsilon \sim 0$ are inserted in the amplitude, obtaining results up to the finite part in ϵ. We find that the form factors F_j^{closed} are finite in ϵ, as expected. In fact, due to the presence of a closed quark loop coupled

to the electroweak bosons, they are proportional to an electroweak coupling factor that is not present at LO. On the contrary, the form factors F_j^{open} contains UV and IR poles, up to order $1/\epsilon^2$ (see section 4 for a discussion on the poles and the extraction of the finite remainder for the amplitude).

The expressions involved in the amplitude are rather large, of the order of hundreds of megabytes, therefore special care must be invested in simplifying these expressions. Since the structure of the poles can be reconstructed starting form LO results thanks to the universal structure of IR singularities, we will focus here on polishing the necessary LO terms, namely the coefficient of ϵ^0, ϵ^1, and ϵ^2, and only the ϵ-finite part of the NLO ones.

First of all, we rescale all dimensionful variables in the form factors by m_V^2, so to obtain

$$F_{j,\epsilon^0}^{\text{class}}(s,t,u,m_h^2,m_V^2) = \left(m_V^2\right)^{-2} \tilde{F}_j^{\text{class}}(T,U,\omega)\,, \tag{3.14}$$

where $s = m_h^2 - t - u$, $T = t/m_V^2$, $U = u/m_V^2$, $\omega = m_h^2/m_V^2$, and the overall m_V^2 factor is obtained by dimensional analysis.

In order to produce manageable expressions we scan each form factor and write it as a sum of algebraic prefactors (expressions containing ratios of polynomials possibly containing square roots) multiplied by transcendental expressions (containing hyperlogarithms, ζ-functions, and π)

$$\tilde{F}_j(T,U,\omega) = \sum_k R_{jk}(T,U,\omega) H_{jk}(T,U,\omega)\,, \tag{3.15}$$

where we dropped the class index for shortness. We find that the simplest part of the amplitude is the LO one ($\tilde{F}_{\epsilon^0}^{\text{open},(1)}$, $\tilde{F}_{\epsilon^1}^{\text{open},(1)}$, $\tilde{F}_{\epsilon^2}^{\text{open},(1)}$), followed by $\tilde{F}_j^{\text{closed}}$, $\tilde{F}_j^{N_c}$, and finally $\tilde{F}_j^{1/N_c}$ as the most complex object of all.

We start by working on the rational prefactors R_{jk}. We apply the functions contained in the Mathematica [55] package MultivariateApart [56] together with their implementation in the computer language Singular [57] to each of the rational prefactors separately, in order to write them as linear combinations of rational expressions M_h without spurious denominators (we name such expressions *rational monomials* from now on)

$$R_{jk}(T,U,\omega) = \sum_h a_{jkh} M_h(T,U,\omega)\,. \tag{3.16}$$

Once the rational prefactors have been decomposed, we follow the ideas described [58] and look for linear relations among them using the rational monomials M_j as independent variables. We stress that in this way we are *not* guaranteed to find all relations among the rational functions, since we are not requesting the partial fraction decomposition to be unique across all rational prefactors. Nevertheless, we find that this procedure is already enough to reduce by about one half the number of independent rational prefactors, see table 3 for a comparison of the size of the form factors at different stages of simplification. Importantly, it has the advantage of not requiring the expensive computation of a Gröbner basis across the full set of denominators that appear in the problem.

As a second step, we look for linear relations among all the rational monomials M_h appearing in each individual rescaled form factor $\tilde{F}$ in order to find a basis of (linearly independent) elements $\overline{M}_h$ for the rational prefactors, obtaining the decomposition

$$R_{jk}(T, U, \omega) = \sum_h \overline{a}_{jkh} \overline{M}_h(T, U, \omega). \tag{3.17}$$

As final step, we search again for relations among different R_{jk} expressed in terms of $\overline{M}_h$, obtaining a basis of rational prefactors. All manipulations are fully analytical and we explicitly check that no more relations arise before moving to a subsequent step in the simplification procedure.

Clearly, we could have in principle omitted the step leading to eq. (3.16). As already stated above, the main reason for this preliminary reduction is that the majority of relations among the R_{jk} are already found without working in the basis $\overline{M}_h$, reducing the number of different M_h to analyze. This is a useful advantage, since the search for linear relations among the M_h is extremely time consuming.

After having simplified the rational prefactors, we move to the combinations of transcendental functions that multiply them. We inspect each term in the sum to check whether it is zero or not. We do it numerically (for different points in the Euclidean or Minkowski region) using the `Mathematica` [55] package `PolyLogTools` [59], and then discard null terms. We then again use these null relations to express hyperlogarithms of higher weight in terms of simpler functions, and we substitute them into the non-zero terms of the amplitude.

Remark. Since we did not use a basis of master integrals with uniform transcendental weight, our initial expressions for the form factors $\tilde{F}_j^{N_c}$ and $\tilde{F}_j^{1/N_c}$ had some contributions with hyperlogarithms of weight 5, which means $n = 5$ in eq. (3.3). Those cancelled after the described simplification of the rational prefactors, leaving only hyperlogarithms of weights ≤ 4. In contrast, the form factors $\tilde{F}_j^{\text{closed}}$ had weight ≤ 4 from the outset.

To conclude, we check numerically for linear relations among the H_k, using the PSLQ algorithm implemented in `Mathematica`. Once all linear relations among the H_k have been applied to the expressions, we check again for relations among the new rational prefactors, to confirm that the expressions cannot be further reduced by means of the techniques described in this section.[3] We stress here that the surviving transcendental expressions are still not in a fully simplified form, and we expect that they can be further optimized both in size and for numerical evaluation by applying the same methods described in [30]. This step is very elaborate due to the large number of different square roots, but it could lead to substantially simpler results. Given its complexity, we leave this analysis for future work.

The expressions for the rescaled form factors $\tilde{F}_i$ presented here (and hence, for the form factors F_i) are valid in all of the three physical regions

$$
\begin{aligned}
0 < m_h^2 < 4m_V^2, && s > m_h^2 && \text{and} && t, u < 0 && \text{for } q\bar{q} \to Hg, \\
0 < m_h^2 < 4m_V^2, && t > m_h^2 && \text{and} && s, u < 0 && \text{for } g\bar{q} \to Hq, \\
0 < m_h^2 < 4m_V^2, && u > m_h^2 && \text{and} && s, t < 0 && \text{for } gq \to H\bar{q},
\end{aligned}
\tag{3.18}
$$

by giving to T, U, and $\omega - T - U$ a small positive imaginary part for analytic continuation.

---

[3]Except for some new zero rational prefactors in $F_2^{\text{open}, 1/N_c}$, no further simplifications happen at this point.

	Original	Partial reduction	Monomial reduction	Basis	No zeroes
$\tilde{F}_{1,\epsilon^0}^{\mathrm{open},(1)}$	8 (31)	7 (31)	7 (24)	6 (24)	6 (24)
$\tilde{F}_{2,\epsilon^0}^{\mathrm{open},(1)}$	8 (33)	7 (33)	7 (30)	6 (30)	5 (24)
$\tilde{F}_{1,\epsilon^1}^{\mathrm{open},(1)}$	23 (70)	18 (70)	18 (50)	12 (50)	9 (21)
$\tilde{F}_{2,\epsilon^1}^{\mathrm{open},(1)}$	22 (58)	16 (58)	16 (43)	12 (43)	9 (22)
$\tilde{F}_{1,\epsilon^2}^{\mathrm{open},(1)}$	45 (87)	26 (87)	26 (65)	17 (65)	12 (37)
$\tilde{F}_{2,\epsilon^2}^{\mathrm{open},(1)}$	44 (73)	23 (73)	23 (58)	17 (58)	10 (22)
$\tilde{E}_1$	46 (45)	22 (45)	22 (28)	15 (28)	10 (17)
$\tilde{E}_2$	46 (45)	22 (45)	22 (28)	15 (28)	10 (17)
$\tilde{F}_{1,\epsilon^0}^{N_c}$	1410 (1454)	234 (1294)	234 (1093)	134 (1093)	100 (983)
$\tilde{F}_{2,\epsilon^0}^{N_c}$	1413 (1389)	213 (1285)	213 (1186)	134 (1186)	117 (1169)
$\tilde{F}_{1,\epsilon^0}^{1/N_c}$	5526 (6789)	1174 (6788)	1100 (5177)	690 (3823)	325 (983)
$\tilde{F}_{2,\epsilon^0}^{1/N_c}$	5524 (5905)	1139 (5894)	1139 (4604)	784 (4517)	460 (1169)
$\tilde{B}_1$	4 (7)	4 (7)	4 (7)	4 (7)	4(7)
$\tilde{B}_2$	4 (7)	4 (7)	4 (7)	4 (7)	4(7)
$\tilde{C}_1$	43 (104)	35 (104)	32 (98)	30 (98)	30 (95)
$\tilde{C}_2$	41 (188)	34 (188)	33 (184)	30 (184)	30 (123)
$\tilde{D}_1$	67 (161)	64 (161)	61 (151)	54 (151)	54 (151)
$\tilde{D}_2$	93 (601)	91 (601)	89 (513)	54 (346)	54 (136)

Table 3. Number of linearly-independent rational prefactors (and rational monomials) at different stages of the reduction procedure. We list the first three non-zero orders $\tilde{A}$ in the ϵ expansion for the LO amplitude, followed by the different component of the two-loop NLO amplitude and then by the different parts of the two-loop finite remainder, without taking into account the part proportional to $\log(m_V^2/\mu_R^2)$ (see section 4).

We kept both of the form factors separately through the simplification process in order to cross check our results thanks to the equivalence between them under the exchange $t \leftrightarrow u$, see (2.24) and (2.26). For size reasons we provide only the first form factor for each component, the second being retrieved by the same exchange.

4 Ultraviolet renormalization and infrared structure

The amplitude contains both ultraviolet and infrared singularities. While UV poles are removed through renormalization, IR singularities cancel only in infrared safe observables.

We remove the UV poles by renormalization of the strong coupling constant α_S in the $\overline{\mathrm{MS}}$ scheme. The NLO renormalization of the strong coupling constant reads [60]

$$\alpha_S = \overline{\alpha}_S\left(\mu_R^2\right) S_\epsilon^{-1} \left(\frac{\mu_R^2}{\mu_0^2}\right)^\epsilon \left[1 - \frac{\overline{\alpha}_S\left(\mu_R^2\right)}{2\pi}\frac{\beta_0}{\epsilon}\right] + O\left(\overline{\alpha}_S^3\left(\mu_R^2\right)\right), \qquad (4.1)$$

where α_S indicates the bare strong coupling constant, $\overline{\alpha}_S\left(\mu_R^2\right)$ the renormalized one, μ_R^2 is the renormalization scale, μ_0^2 is the dimensional regularization scale, $S_\epsilon = (4\pi)^\epsilon \mathrm{e}^{-\epsilon\gamma}$, with

γ being the Euler-Mascheroni constant, and

$$\beta_0 = \frac{11C_A - 4N_f T_R}{6}\,, \tag{4.2}$$

with $C_A = N_c$, $T_R = 1/2$, and N_f the number of active flavors. From now on, we fix $\mu_0 = \mu_R$ for definiteness.

We provide our results for the $\overline{\text{MS}}$-renormalized form factors $\mathcal{F}_j^{\text{class}}$ as a series expansion in the renormalized strong coupling constant as follows

$$
\begin{aligned}
\mathcal{F}_j^{\text{open}} &= S_\epsilon \sqrt{\frac{\overline{\alpha}_S\left(\mu_R^2\right)}{S_\epsilon}} \left[\mathcal{F}_j^{\text{open},(1)} + \left(\frac{\overline{\alpha}_S\left(\mu_R^2\right)}{2\pi} \right) \mathcal{F}_j^{\text{open},(2)} + \mathcal{O}\left(\overline{\alpha}_S^2\right) \right], \\
\mathcal{F}_j^{\text{closed}} &= S_\epsilon \sqrt{\frac{\overline{\alpha}_S\left(\mu_R^2\right)}{S_\epsilon}} \left[\left(\frac{\overline{\alpha}_S\left(\mu_R^2\right)}{2\pi} \right) \mathcal{F}_j^{\text{closed},(2)} + \mathcal{O}\left(\overline{\alpha}_S^2\right) \right],
\end{aligned}
\tag{4.3}
$$

where the coefficients read

$$
\begin{aligned}
\mathcal{F}_j^{\text{open},(1)} &= S_\epsilon^{-1} F_j^{\text{open},(1)}\,, \\
\mathcal{F}_j^{\text{open},(2)} &= S_\epsilon^{-2} F_j^{\text{open},(2)} - S_\epsilon^{-1} \frac{\beta_0}{2\epsilon} F_j^{\text{open},(1)}\,, \\
\mathcal{F}_j^{\text{closed},(2)} &= S_\epsilon^{-2} F_j^{\text{closed},(2)}\,,
\end{aligned}
\tag{4.4}
$$

and the dependence of the form factors on the vector boson mass m_V is left implicit from now on for ease of notation.[4] After UV renomalisation, $\mathcal{F}^{\text{open},(2)}$ still contains IR poles. The structure of such singularities for QCD virtual NLO corrections is well-known and is fully captured by Catani's operator $\mathbf{I}^{(1)}$ [60]. We define therefore the finite reminders as

$$\mathcal{F}_j^{\text{open},(2)} = \mathbf{I}^{(1)} \mathcal{F}_j^{\text{open},(1)} + \mathcal{F}_{j,\text{fin}}^{\text{open},(2)}\,, \quad \mathcal{F}_j^{\text{closed},(2)} = \mathcal{F}_{j,\text{fin}}^{\text{closed},(2)} \tag{4.5}$$

where Catani's operator $\mathbf{I}^{(1)}$ reads

$$
\begin{aligned}
\mathbf{I}^{(1)} = -\frac{1}{2} \frac{e^{\epsilon\gamma}}{\Gamma(1-\epsilon)} &\left\{ \mathcal{V}_q^{\text{sing}}(\epsilon) \frac{2C_F - C_A}{C_F} \left(-\frac{\mu_R^2}{s} \right)^\epsilon + \right. \\
&\left. + \frac{1}{2} \left(\mathcal{V}_g^{\text{sing}}(\epsilon) + \frac{C_A}{C_F} \mathcal{V}_q^{\text{sing}}(\epsilon) \right) \left[\left(-\frac{\mu_R^2}{t} \right)^\epsilon + \left(-\frac{\mu_R^2}{u} \right)^\epsilon \right] \right\},
\end{aligned}
\tag{4.6}
$$

where the Mandelstam invariants carry an implicit small positive imaginary part, $C_F = (N_c^2 - 1)/(2N_c)$, and

$$\mathcal{V}_q^{\text{sing}}(\epsilon) = \frac{C_F}{\epsilon^2} + \frac{3C_F}{2\epsilon}\,, \tag{4.7}$$

$$\mathcal{V}_g^{\text{sing}}(\epsilon) = \frac{C_A}{\epsilon^2} + \frac{11C_A - 2N_f}{6\epsilon}\,. \tag{4.8}$$

In order to construct the finite remainders $\mathcal{F}_{\text{fin}}^{\text{open},(2)}$ we also require the one-loop results, $\mathcal{F}_{\text{fin}}^{\text{open},(1)}$, up to order ϵ^2. To compute it, we use the same projectors and techniques

[4]We stress that the extra factor of S_ϵ in eqs. (4.3) is chosen to reabsorb the terms proportional to γ and $\log(4\pi)$ coming from the loop integration on the electroweak vector bosons.

	Hyperlogarithms	Weight	Size
$\tilde{A}_{\epsilon^0}$	11	1 to 2	0.5 kiB
$\tilde{A}_{\epsilon^1}$	82	1 to 3	3.1 kiB
$\tilde{A}_{\epsilon^2}$	386	1 to 4	16.7 kiB
$\tilde{B}_1$	11	2 to 3	1.7 kiB
$\tilde{C}_1$	6907	1 to 4	0.7 MiB
$\tilde{D}_1$	16 755	1 to 4	1.3 MiB
$\tilde{E}_1$	292	0 to 4	16.6 kiB

Table 4. The complexity of our final expressions for the LO, and NLO finite remainder. The second column shows the number of different hyperlogarithm functions that appear.

illustrated in section 2 and we compute the one-loop master integrals by direct integration over Feynman-Schwinger parameters. We provide the set of propagators and the master integrals for the one-loop case in appendix A. We have checked numerically that the ϵ-pole structures of $\mathcal{F}_j^{\mathrm{open},(2)}$ and $\mathbf{I}^{(1)}\mathcal{F}_j^{\mathrm{open},(1)}$ agree, in different points in Euclidean and Minkowski regions, using Ginac [61] and PolyLogTools [59].

After all these manipulations, the one-loop and two-loop finite reminders can be decomposed as a polynomial in N_c and N_f. To simplify the notation and present our results we write

$$\mathcal{F}_{j,\mathrm{fin}}^{\mathrm{open},(1)} = A_j\,, \quad \mathcal{F}_{j,\mathrm{fin}}^{\mathrm{open},(2)} = N_f B_j + N_c C_j + \frac{1}{N_c}D_j\,, \quad \mathcal{F}_{j,\mathrm{fin}}^{\mathrm{closed},(2)} = E_j\,. \tag{4.9}$$

We apply the same simplification procedure illustrated in section 3 to the finite remainder as well (see table 3 and table 4 for the details). We provide the analytical expressions for the coefficients A_1, B_1, C_1, D_1, E_1 (which have transcendental weight up to four), keeping the scale μ_R^2 general, as supplementary material attached to this paper. As discussed in eq. (2.24) and (2.26), the remaining form factor can be obtained by exchanging $t \leftrightarrow u$.

For reference, in table 5 we provide numerical values for the coefficients listed in eq. (4.9) evaluated at the points

$$
\begin{aligned}
P_{q\bar{q}} &= \{\, s \to +375.1\,\mathrm{GeV}\,, & t \to -100.0\,\mathrm{GeV}\,, & \quad u \to -150.0\,\mathrm{GeV}\,\}\,, \\
P_{qg} &= \{\, s \to -150.0\,\mathrm{GeV}\,, & t \to +375.1\,\mathrm{GeV}\,, & \quad u \to -100.0\,\mathrm{GeV}\,\}\,, \\
P_{\bar{q}g} &= \{\, s \to -100.0\,\mathrm{GeV}\,, & t \to -150.0\,\mathrm{GeV}\,, & \quad u \to +375.1\,\mathrm{GeV}\,\}\,,
\end{aligned}
\tag{4.10}
$$

with $\mu_R = m_h = 125.1\,\mathrm{GeV}$ and $m_V = m_W = 80.4\,\mathrm{GeV}$.

5 Conclusions

In this paper, we computed the helicity amplitudes for the two-loop mixed QCD-Electroweak corrections to Higgs plus ject production in the quark-initiate channels qg, $\bar{q}g$, and $q\bar{q}$, keeping full dependence on the Higgs and EW vector boson masses. These amplitudes are the last missing ingredient, together with the $ggHg$ expressions computed in [30, 31], to

	$P_{q\bar{q}}$	P_{qg}	$P_{\bar{q}g}$
$\tilde{A}_{1,\epsilon^0}$	$+0.33014631$	$+0.07937750 + 0.56737915\,\mathrm{i}$	$-0.20133007 + 0.56797218\,\mathrm{i}$
$\tilde{A}_{1,\epsilon^1}$	$+0.86304102$	$-0.29185479 + 1.53102839\,\mathrm{i}$	$-1.22164117 + 0.87055442\,\mathrm{i}$
$\tilde{A}_{1,\epsilon^2}$	$+1.28181266$	$-1.04954624 + 1.96804187\,\mathrm{i}$	$-1.87982473 + 0.03486591\,\mathrm{i}$
$\tilde{B}_1$	-0.00116710	$+0.15432174 + 0.02054956\,\mathrm{i}$	$+0.12722625 + 0.11327291\,\mathrm{i}$
$\tilde{C}_1$	$+0.51514217 + 0.00193541\,\mathrm{i}$	$-0.26266335 - 0.57780014\,\mathrm{i}$	$-0.49525929 - 1.62795284\,\mathrm{i}$
$\tilde{D}_1$	$+0.96451329 + 0.74965721\,\mathrm{i}$	$+1.25415918 + 0.18720716\,\mathrm{i}$	$-1.20060441 + 0.68012840\,\mathrm{i}$
$\tilde{E}_1$	$-0.11645020 - 0.21841056\,\mathrm{i}$	$+0.51765798 + 0.00588251\,\mathrm{i}$	$+0.85351666 + 0.01089854\,\mathrm{i}$

Table 5. Numerical values of the different parts of the LO and NLO form factors, evaluated at points defined in eq. (4.10).

construct electroweak corrections to Higgs plus jet production at hadron colliders. Starting from the Feynman diagrams contributing to the process we extracted the form factors by means of projectors and subsequently build the independent helicity amplitudes as a linear combination of scalar two-loop Feynman integrals. We use IBP relations to write the form factors as linear combinations of master integrals, which we subsequently evaluate by direct integration over Feynman/Schwinger parameters using the public code `HyperInt`, exploiting their property of linearly reducibility. We simplify the outcome by separating the algebraic prefactors from the transcendental functions and rewriting the first ones in terms of a basis of linearly independent prefactors, while the transcendental expressions are investigated numerically to remove any linearly-dependent or zero term by means of the PSLQ algorithm. The result is formally more compact and reduces the number of transcendental functions to be evaluated to obtain numerical results. As a byproduct we also obtained expressions for the leading order one-loop form factors up to order ϵ^2, necessary to verify the UV-renormalized IR pole structure described by the Catani's operator.

The computation described here shares many formal similarities with the $ggHg$ case discussed in [30], although being much more challenging on a practical level. The main reason for this is the fact that we are considering a NLO computation with a nonzero ϵ-pole structure, that requires the evaluation of a larger number of master integrals, with more complex topologies and up to higher order in the ϵ expansion. The complexity and size of the ϵ^0 results required additional refinement, obtained through the reduction to a basis of rational prefactors and the implementation of linear relations among the transcendental expressions obtained through PLSQ. While the results presented here are not optimised for fast numerical evaluation due to the complexity of the alphabet involved, they can be evaluated straightforwardly in all relevant kinematical regions by specifying a suitable imaginary part for all kinematical invariants. Moreover, they can be used as a starting point for the construction of a optimised analytic expressions in the various kinematical regions, for example following the ideas described in [62] and already used in for example in [30]. We leave this non-trivial step for a future investigation.

Denominator	Integral family LO
D_1	$k^2 - m_V^2$
D_2	$(k - p_1 - p_2 - p_3)^2 - m_V^2$
D_3	$(k - p_2 - p_3)^2$
D_4	$(k - p_2)^2$

Table 6. Definition of the LO integral family LO. The loop momentum is denoted by k. m_V indicates the mass of the vector boson. The prescription $+i\epsilon$ is understood for each propagator and not written explicitly.

Acknowledgments

A The master integrals

A.1 LO amplitude and master integrals

The LO amplitude consists of 3 Feynman diagrams, whose sum can be expressed in terms of 5 master integrals (modulus permutation of the external legs). We proceed in the same way as for the virtual NLO amplitude, see section 2 and section 3. The propagators of the integral family LO are listed in table 6. The Symanzik polynomials are

$$\mathcal{U} = x_1 + x_2 + x_3 + x_4 \quad \text{and} \quad \mathcal{F} = -m_h^2 x_1 x_2 - t x_2 x_4 - u x_1 x_3 + m_V^2 (x_1 + x_2)\mathcal{U}.$$

As master integrals, we have chosen

$$\mathcal{I}_{\mathsf{LO}}(3,0,0,0)\,, \quad \mathcal{I}_{\mathsf{LO}}(2,1,0,0)\,, \quad \mathcal{I}_{\mathsf{LO}}^{(6)}(2,0,2,0)\,, \quad \mathcal{I}_{\mathsf{LO}}^{(6)}(2,2,1,0)\,, \quad \mathcal{I}_{\mathsf{LO}}^{(6)}(1,1,1,1)\,. \tag{A.1}$$

The integrals with an upper index (6) are evaluated in $d = 6 - 2\epsilon$ dimensions (without any upper index: in $d = 4 - 2\epsilon$).

A.2 Virtual NLO master integrals

We expressed the NLO virtual amplitude in terms of 93 master integrals (modulo permutations of the external legs). In particular

- the planar integral family PL has four maximal topologies (T_3–T_6 in figure 2),

$$\mathcal{I}_{\mathsf{PL}}(1,1,1,1,1,1,1,0,0)\,, \qquad \mathcal{I}_{\mathsf{PL}}(0,1,1,1,1,1,1,1,0)\,,$$
$$\mathcal{I}_{\mathsf{PL}}(1,1,1,1,0,0,1,1,1)\,, \qquad \mathcal{I}_{\mathsf{PL}}(0,1,1,1,1,0,1,1,1)\,,$$

and contains 70 master integrals

$$
\begin{array}{lll}
\mathcal{I}_{\mathsf{PL}}^{(6)}(0,0,0,2,0,2,2,2,0)\,, & \mathcal{I}_{\mathsf{PL}}(0,0,1,2,0,0,2,0,0)\,, & \mathcal{I}_{\mathsf{PL}}^{(6)}(0,0,2,0,0,2,1,2,0)\,, \\
\mathcal{I}_{\mathsf{PL}}^{(6)}(0,0,2,0,1,1,2,1,0)\,, & \mathcal{I}_{\mathsf{PL}}^{(6)}(0,0,2,0,2,0,2,1,0)\,, & \mathcal{I}_{\mathsf{PL}}(0,0,2,2,0,0,1,0,0)\,, \\
\mathcal{I}_{\mathsf{PL}}^{(6)}(0,0,3,0,0,2,0,2,0)\,, & \mathcal{I}_{\mathsf{PL}}(0,1,1,0,1,1,1,0,0)\,, & \mathcal{I}_{\mathsf{PL}}(0,1,1,1,0,1,0,1,0)\,, \\
\mathcal{I}_{\mathsf{PL}}(0,1,1,1,0,1,1,0,0)\,, & \mathcal{I}_{\mathsf{PL}}^{(6)}(0,1,1,1,1,1,1,2,0)\,, & \mathcal{I}_{\mathsf{PL}}^{(6)}(0,1,1,1,1,1,2,1,0)\,, \\
\mathcal{I}_{\mathsf{PL}}^{(6)}(0,1,2,0,0,2,0,0,0)\,, & \mathcal{I}_{\mathsf{PL}}^{(6)}(0,1,2,0,0,2,2,1,0)\,, & \mathcal{I}_{\mathsf{PL}}(0,1,2,0,1,0,1,0,0)\,, \\
\mathcal{I}_{\mathsf{PL}}(0,1,2,0,2,0,0,0,0)\,, & \mathcal{I}_{\mathsf{PL}}^{(6)}(0,1,2,0,2,0,2,1,0)\,, & \mathcal{I}_{\mathsf{PL}}(0,1,2,1,0,0,1,0,0)\,, \\
\mathcal{I}_{\mathsf{PL}}(0,1,2,1,0,1,0,0,0)\,, & \mathcal{I}_{\mathsf{PL}}^{(6)}(0,1,2,2,0,0,2,0,1)\,, & \mathcal{I}_{\mathsf{PL}}(0,2,0,2,0,1,0,0,0)\,, \\
\mathcal{I}_{\mathsf{PL}}(0,2,0,2,0,1,1,0,0)\,, & \mathcal{I}_{\mathsf{PL}}^{(6)}(0,2,0,2,0,2,2,1,0)\,, & \mathcal{I}_{\mathsf{PL}}(0,2,1,1,0,1,1,0,0)\,, \\
\mathcal{I}_{\mathsf{PL}}^{(6)}(0,2,1,1,1,1,1,0,0)\,, & \mathcal{I}_{\mathsf{PL}}^{(6)}(0,2,1,1,1,1,1,1,0)\,, & \mathcal{I}_{\mathsf{PL}}^{(6)}(0,2,1,1,1,1,2,0,0)\,, \\
\mathcal{I}_{\mathsf{PL}}(0,2,2,0,0,1,0,0,0)\,, & \mathcal{I}_{\mathsf{PL}}^{(6)}(0,2,2,0,0,2,0,1,0)\,, & \mathcal{I}_{\mathsf{PL}}^{(6)}(0,2,2,0,0,2,0,1,1)\,, \\
\mathcal{I}_{\mathsf{PL}}(0,2,2,0,1,0,0,0,0)\,, & \mathcal{I}_{\mathsf{PL}}(0,2,2,0,1,0,1,0,0)\,, & \mathcal{I}_{\mathsf{PL}}^{(6)}(0,2,2,0,1,1,0,1,0)\,, \\
\mathcal{I}_{\mathsf{PL}}^{(6)}(0,2,2,0,1,1,1,1,0)\,, & \mathcal{I}_{\mathsf{PL}}^{(6)}(0,2,2,0,2,0,1,1,0)\,, & \mathcal{I}_{\mathsf{PL}}(0,2,2,1,0,0,1,0,0)\,, \\
\mathcal{I}_{\mathsf{PL}}(0,2,2,1,0,1,0,0,0)\,, & \mathcal{I}_{\mathsf{PL}}^{(6)}(0,2,2,1,0,1,1,0,0)\,, & \mathcal{I}_{\mathsf{PL}}^{(6)}(0,2,2,1,1,0,1,0,0)\,, \\
\mathcal{I}_{\mathsf{PL}}^{(6)}(0,2,2,2,0,0,1,0,1)\,, & \mathcal{I}_{\mathsf{PL}}^{(6)}(0,3,1,1,1,1,0,0,0)\,, & \mathcal{I}_{\mathsf{PL}}^{(6)}(0,3,1,1,1,1,1,0,0)\,, \\
\mathcal{I}_{\mathsf{PL}}^{(6)}(0,3,2,0,1,1,0,1,0)\,, & \mathcal{I}_{\mathsf{PL}}^{(6)}(0,3,2,1,1,0,1,0,0)\,, & \mathcal{I}_{\mathsf{PL}}^{(6)}(0,4,1,1,1,1,0,0,0)\,, \\
\mathcal{I}_{\mathsf{PL}}(1,0,1,0,1,0,2,0,0)\,, & \mathcal{I}_{\mathsf{PL}}^{(6)}(1,0,1,1,1,0,3,0,0)\,, & \mathcal{I}_{\mathsf{PL}}^{(6)}(1,0,1,1,1,0,4,0,0)\,, \\
\mathcal{I}_{\mathsf{PL}}(1,0,2,0,1,0,2,0,0)\,, & \mathcal{I}_{\mathsf{PL}}^{(6)}(1,0,2,1,0,0,2,0,1)\,, & \mathcal{I}_{\mathsf{PL}}^{(6)}(1,0,2,1,0,0,3,0,1)\,, \\
\mathcal{I}_{\mathsf{PL}}(1,1,1,0,0,1,1,0,0)\,, & \mathcal{I}_{\mathsf{PL}}(1,1,1,0,1,0,1,0,0)\,, & \mathcal{I}_{\mathsf{PL}}(1,1,1,0,1,0,2,0,0)\,, \\
\mathcal{I}_{\mathsf{PL}}(1,1,1,0,1,1,1,0,0)\,, & \mathcal{I}_{\mathsf{PL}}(1,1,1,1,0,0,1,0,0)\,, & \mathcal{I}_{\mathsf{PL}}(1,1,1,1,0,1,1,0,0)\,, \\
\mathcal{I}_{\mathsf{PL}}^{(6)}(1,1,1,1,1,0,2,0,0)\,, & \mathcal{I}_{\mathsf{PL}}^{(6)}(1,1,1,1,1,0,3,0,0)\,, & \mathcal{I}_{\mathsf{PL}}^{(6)}(1,1,2,0,1,0,2,0,0)\,, \\
\mathcal{I}_{\mathsf{PL}}^{(6)}(1,1,2,1,0,0,2,0,1)\,, & \mathcal{I}_{\mathsf{PL}}(1,2,1,0,0,0,0,0,0)\,, & \mathcal{I}_{\mathsf{PL}}^{(6)}(1,2,1,1,1,0,2,0,0)\,, \\
\mathcal{I}_{\mathsf{PL}}^{(6)}(2,0,2,0,0,0,2,1,0)\,, & \mathcal{I}_{\mathsf{PL}}^{(6)}(2,0,2,0,0,0,2,1,1)\,, & \mathcal{I}_{\mathsf{PL}}(2,1,1,0,0,0,2,0,0)\,, \\
\mathcal{I}_{\mathsf{PL}}^{(6)}(2,1,2,0,0,0,2,1,0)\,, & \mathcal{I}_{\mathsf{PL}}^{(6)}(2,1,2,0,0,0,2,1,1)\,, & \mathcal{I}_{\mathsf{PL}}(2,2,0,0,1,0,0,0,0)\,, \\
& \mathcal{I}_{\mathsf{PL}}(2,2,0,0,1,0,1,0,0)\,; & \mathrm{(A.2)}
\end{array}
$$

- the integral family NA (with maximal topology $\mathcal{I}_{\mathsf{NA}}(1,1,1,1,1,1,1,0,0)$, T_2 in figure 2) contains 18 master integrals:

$$\mathcal{I}_{\mathsf{NA}}^{(6)}(0,1,1,0,1,3,1,0,0)\,, \quad \mathcal{I}_{\mathsf{NA}}^{(6)}(0,1,1,1,1,2,1,0,0)\,, \quad \mathcal{I}_{\mathsf{NA}}^{(6)}(0,1,1,2,1,1,1,0,0)\,,$$
$$\mathcal{I}_{\mathsf{NA}}^{(6)}(0,1,1,2,1,2,1,0,0)\,, \quad \mathcal{I}_{\mathsf{NA}}^{(6)}(0,1,1,3,1,0,1,0,0)\,, \quad \mathcal{I}_{\mathsf{NA}}^{(6)}(0,1,1,4,1,0,1,0,0)\,,$$
$$\mathcal{I}_{\mathsf{NA}}(1,1,0,1,1,0,1,0,0)\,, \quad \mathcal{I}_{\mathsf{NA}}(1,1,0,1,1,1,1,0,0)\,, \quad \mathcal{I}_{\mathsf{NA}}^{(6)}(1,1,1,0,0,3,1,0,0)\,,$$
$$\mathcal{I}_{\mathsf{NA}}^{(6)}(1,1,1,0,0,4,1,0,0)\,, \quad \mathcal{I}_{\mathsf{NA}}^{(6)}(1,1,1,1,0,2,1,0,0)\,, \quad \mathcal{I}_{\mathsf{NA}}^{(6)}(1,1,1,1,1,2,1,0,0)\,,$$
$$\mathcal{I}_{\mathsf{NA}}^{(6)}(1,1,1,1,1,3,1,0,0)\,, \quad \mathcal{I}_{\mathsf{NA}}^{(6)}(1,1,1,2,0,1,1,0,0)\,, \quad \mathcal{I}_{\mathsf{NA}}^{(6)}(1,1,1,2,0,2,1,0,0)\,,$$
$$\mathcal{I}_{\mathsf{NA}}^{(6)}(1,1,1,2,1,1,1,0,0)\,, \quad \mathcal{I}_{\mathsf{NA}}^{(6)}(1,1,1,3,0,0,1,0,0)\,, \quad \mathcal{I}_{\mathsf{NA}}^{(6)}(1,1,1,3,1,1,1,0,0)\,; \tag{A.3}$$

- the integral family NB (with maximal topology $\mathcal{I}_{\mathsf{NB}}(1,1,1,1,0,1,1,1,0)$, T_1 in figure 2) contains 5 master integrals:

$$\mathcal{I}_{\mathsf{NB}}^{(6)}(1,1,1,0,0,3,1,1,0)\,, \quad \mathcal{I}_{\mathsf{NB}}^{(6)}(1,1,1,1,0,3,1,1,0)\,, \quad \mathcal{I}_{\mathsf{NB}}^{(6)}(1,1,1,2,0,2,1,1,0)\,,$$
$$\mathcal{I}_{\mathsf{NB}}^{(6)}(1,1,1,3,0,0,1,1,0)\,, \quad\quad\quad\quad\quad\quad\quad\quad\quad\quad \mathcal{I}_{\mathsf{NB}}^{(6)}(1,1,1,3,0,1,1,1,0)\,. \tag{A.4}$$

The integrals with an upper index (6) are evaluated in $d = 6 - 2\epsilon$ dimensions (without any upper index: in $d = 4 - 2\epsilon$).

Open Access. This article is distributed under the terms of the Creative Commons Attribution License ([CC-BY 4.0](#)), which permits any use, distribution and reproduction in any medium, provided the original author(s) and source are credited.

References

[1] ATLAS collaboration, *Observation of a new particle in the search for the Standard Model Higgs boson with the ATLAS detector at the LHC*, *Phys. Lett. B* **716** (2012) 1 [`arXiv:1207.7214`] [INSPIRE].

[2] CMS collaboration, *Observation of a New Boson at a Mass of* 125 *GeV with the CMS Experiment at the LHC*, *Phys. Lett. B* **716** (2012) 30 [`arXiv:1207.7235`] [INSPIRE].

[3] A. Dainese, M. Mangano, A.B. Meyer, A. Nisati, G. Salam and M.A. Vesterinen, eds., *Report on the Physics at the HL-LHC,and Perspectives for the HE-LHC*, vol. 7/2019 of *CERN Yellow Rep. Monogr.*, CERN, Geneva, Switzerland (2019) [CYRM-2019-007].

[4] ATLAS collaboration, *Luminosity determination in pp collisions at* $\sqrt{s} = 13$ *TeV using the ATLAS detector at the LHC*, ATLAS-CONF-2019-021 (2019).

[5] CMS collaboration, *Precision luminosity measurement in proton-proton collisions at* $\sqrt{s} = 13$ *TeV in 2015 and 2016 at CMS*, *Eur. Phys. J. C* **81** (2021) 800 [`arXiv:2104.01927`] [INSPIRE].

[6] CMS collaboration, *Jet energy scale and resolution in the CMS experiment in pp collisions at* 8 *TeV*, 2017 *JINST* **12** P02014 [`arXiv:1607.03663`] [INSPIRE].

[7] ATLAS collaboration, *Jet energy scale measurements and their systematic uncertainties in proton-proton collisions at $\sqrt{s} = 13$ TeV with the ATLAS detector*, *Phys. Rev. D* **96** (2017) 072002 [arXiv:1703.09665] [INSPIRE].

[8] F. Bishara, U. Haisch, P.F. Monni and E. Re, *Constraining Light-Quark Yukawa Couplings from Higgs Distributions*, *Phys. Rev. Lett.* **118** (2017) 121801 [arXiv:1606.09253] [INSPIRE].

[9] H.M. Georgi, S.L. Glashow, M.E. Machacek and D.V. Nanopoulos, *Higgs Bosons from Two Gluon Annihilation in Proton Proton Collisions*, *Phys. Rev. Lett.* **40** (1978) 692 [INSPIRE].

[10] D. Graudenz, M. Spira and P.M. Zerwas, *QCD corrections to Higgs boson production at proton proton colliders*, *Phys. Rev. Lett.* **70** (1993) 1372 [INSPIRE].

[11] M. Spira, A. Djouadi, D. Graudenz and P.M. Zerwas, *Higgs boson production at the LHC*, *Nucl. Phys. B* **453** (1995) 17 [hep-ph/9504378] [INSPIRE].

[12] U. Aglietti, R. Bonciani, G. Degrassi and A. Vicini, *Analytic Results for Virtual QCD Corrections to Higgs Production and Decay*, *JHEP* **01** (2007) 021 [hep-ph/0611266] [INSPIRE].

[13] M.L. Czakon and M. Niggetiedt, *Exact quark-mass dependence of the Higgs-gluon form factor at three loops in QCD*, *JHEP* **05** (2020) 149 [arXiv:2001.03008] [INSPIRE].

[14] C. Anastasiou, C. Duhr, F. Dulat, F. Herzog and B. Mistlberger, *Higgs Boson Gluon-Fusion Production in QCD at Three Loops*, *Phys. Rev. Lett.* **114** (2015) 212001 [arXiv:1503.06056] [INSPIRE].

[15] B. Mistlberger, *Higgs boson production at hadron colliders at N^3LO in QCD*, *JHEP* **05** (2018) 028 [arXiv:1802.00833] [INSPIRE].

[16] C. Anastasiou et al., *High precision determination of the gluon fusion Higgs boson cross-section at the LHC*, *JHEP* **05** (2016) 058 [arXiv:1602.00695] [INSPIRE].

[17] G. Degrassi and F. Maltoni, *Two-loop electroweak corrections to Higgs production at hadron colliders*, *Phys. Lett. B* **600** (2004) 255 [hep-ph/0407249] [INSPIRE].

[18] U. Aglietti, R. Bonciani, G. Degrassi and A. Vicini, *Two loop light fermion contribution to Higgs production and decays*, *Phys. Lett. B* **595** (2004) 432 [hep-ph/0404071] [INSPIRE].

[19] U. Aglietti and R. Bonciani, *Master integrals with 2 and 3 massive propagators for the 2 loop electroweak form-factor — planar case*, *Nucl. Phys. B* **698** (2004) 277 [hep-ph/0401193] [INSPIRE].

[20] U. Aglietti, R. Bonciani, L. Grassi and E. Remiddi, *The Two loop crossed ladder vertex diagram with two massive exchanges*, *Nucl. Phys. B* **789** (2008) 45 [arXiv:0705.2616] [INSPIRE].

[21] R. Bonciani, A. Ferroglia, P. Mastrolia, E. Remiddi and J.J. van der Bij, *Planar box diagram for the $(N_F = 1)$ two loop QED virtual corrections to Bhabha scattering*, *Nucl. Phys. B* **681** (2004) 261 [*Erratum ibid.* **702** (2004) 364] [hep-ph/0310333] [INSPIRE].

[22] R. Bonciani, P. Mastrolia and E. Remiddi, *Vertex diagrams for the QED form-factors at the two loop level*, *Nucl. Phys. B* **661** (2003) 289 [*Erratum ibid.* **702** (2004) 359] [hep-ph/0301170] [INSPIRE].

[23] R. Bonciani, A. Ferroglia, T. Gehrmann, D. Maître and C. Studerus, *Two-Loop Fermionic Corrections to Heavy-Quark Pair Production: The Quark-Antiquark Channel*, *JHEP* **07** (2008) 129 [arXiv:0806.2301] [INSPIRE].

[24] R. Bonciani, A. Ferroglia, T. Gehrmann and C. Studerus, *Two-Loop Planar Corrections to Heavy-Quark Pair Production in the Quark-Antiquark Channel*, *JHEP* **08** (2009) 067 [arXiv:0906.3671] [INSPIRE].

[25] M. Bonetti, K. Melnikov and L. Tancredi, *Two-loop electroweak corrections to Higgs-gluon couplings to higher orders in the dimensional regularization parameter*, *Nucl. Phys. B* **916** (2017) 709 [arXiv:1610.05497] [INSPIRE].

[26] C. Anastasiou, R. Boughezal and F. Petriello, *Mixed QCD-electroweak corrections to Higgs boson production in gluon fusion*, *JHEP* **04** (2009) 003 [arXiv:0811.3458] [INSPIRE].

[27] M. Bonetti, K. Melnikov and L. Tancredi, *Three-loop mixed QCD-electroweak corrections to Higgs boson gluon fusion*, *Phys. Rev. D* **97** (2018) 034004 [arXiv:1711.11113] [INSPIRE].

[28] M. Bonetti, K. Melnikov and L. Tancredi, *Higher order corrections to mixed QCD-EW contributions to Higgs boson production in gluon fusion*, *Phys. Rev. D* **97** (2018) 056017 [*Erratum ibid.* **97** (2018) 099906] [arXiv:1801.10403] [INSPIRE].

[29] M. Becchetti, R. Bonciani, V. Casconi, V. Del Duca and F. Moriello, *Planar master integrals for the two-loop light-fermion electroweak corrections to Higgs plus jet production*, *JHEP* **12** (2018) 019 [arXiv:1810.05138] [INSPIRE].

[30] M. Bonetti, E. Panzer, V.A. Smirnov and L. Tancredi, *Two-loop mixed QCD-EW corrections to $gg \to Hg$*, *JHEP* **11** (2020) 045 [arXiv:2007.09813] [INSPIRE].

[31] M. Becchetti, R. Bonciani, V. Del Duca, V. Hirschi, F. Moriello and A. Schweitzer, *Next-to-leading order corrections to light-quark mixed QCD-EW contributions to Higgs boson production*, *Phys. Rev. D* **103** (2021) 054037 [arXiv:2010.09451] [INSPIRE].

[32] M. Becchetti, F. Moriello and A. Schweitzer, *Two-loop amplitude for mixed QCD-EW corrections to $gg \to Hg$*, *JHEP* **04** (2022) 139 [arXiv:2112.07578] [INSPIRE].

[33] W.-Y. Keung and F.J. Petriello, *Electroweak and finite quark-mass effects on the Higgs boson transverse momentum distribution*, *Phys. Rev. D* **80** (2009) 013007 [arXiv:0905.2775] [INSPIRE].

[34] V. Hirschi, S. Lionetti and A. Schweitzer, *One-loop weak corrections to Higgs production*, *JHEP* **05** (2019) 002 [arXiv:1902.10167] [INSPIRE].

[35] F. Brown, *The Massless higher-loop two-point function*, *Commun. Math. Phys.* **287** (2009) 925 [arXiv:0804.1660] [INSPIRE].

[36] F.C.S. Brown, *On the periods of some Feynman integrals*, arXiv:0910.0114 [INSPIRE].

[37] E. Panzer, *Algorithms for the symbolic integration of hyperlogarithms with applications to Feynman integrals*, *Comput. Phys. Commun.* **188** (2015) 148 [arXiv:1403.3385] [INSPIRE].

[38] J.C. Romao and J.P. Silva, *A resource for signs and Feynman diagrams of the Standard Model*, *Int. J. Mod. Phys. A* **27** (2012) 1230025 [arXiv:1209.6213] [INSPIRE].

[39] K. Melnikov, L. Tancredi and C. Wever, *Two-loop amplitudes for $qg \to Hq$ and $q\bar{q} \to Hg$ mediated by a nearly massless quark*, *Phys. Rev. D* **95** (2017) 054012 [arXiv:1702.00426] [INSPIRE].

[40] F. Buccioni et al., *OpenLoops 2*, *Eur. Phys. J. C* **79** (2019) 866 [arXiv:1907.13071] [INSPIRE].

[41] P. Nogueira, *Automatic Feynman graph generation*, *J. Comput. Phys.* **105** (1993) 279 [INSPIRE].

[42] B. Ruijl, T. Ueda and J. Vermaseren, *FORM version 4.2*, arXiv:1707.06453 [ɪɴSPIRE].

[43] J. Kuipers, T. Ueda and J.A.M. Vermaseren, *Code Optimization in FORM*, *Comput. Phys. Commun.* **189** (2015) 1 [arXiv:1310.7007] [ɪɴSPIRE].

[44] F.V. Tkachov, *A Theorem on Analytical Calculability of Four Loop Renormalization Group Functions*, *Phys. Lett. B* **100** (1981) 65 [ɪɴSPIRE].

[45] K.G. Chetyrkin and F.V. Tkachov, *Integration by Parts: The Algorithm to Calculate β-functions in 4 Loops*, *Nucl. Phys. B* **192** (1981) 159 [ɪɴSPIRE].

[46] S. Laporta, *High precision calculation of multiloop Feynman integrals by difference equations*, *Int. J. Mod. Phys. A* **15** (2000) 5087 [hep-ph/0102033] [ɪɴSPIRE].

[47] C. Studerus, *Reduze-Feynman Integral Reduction in C++*, *Comput. Phys. Commun.* **181** (2010) 1293 [arXiv:0912.2546] [ɪɴSPIRE].

[48] A. von Manteuffel and C. Studerus, *Reduze 2 — Distributed Feynman Integral Reduction*, arXiv:1201.4330 [ɪɴSPIRE].

[49] P. Maierhöfer, J. Usovitsch and P. Uwer, *Kira — A Feynman integral reduction program*, *Comput. Phys. Commun.* **230** (2018) 99 [arXiv:1705.05610] [ɪɴSPIRE].

[50] V.A. Smirnov, *Analytic tools for Feynman integrals*, *Springer Tracts Mod. Phys.* **250** (2012) 1 [ɪɴSPIRE].

[51] E. Remiddi and J.A.M. Vermaseren, *Harmonic polylogarithms*, *Int. J. Mod. Phys. A* **15** (2000) 725 [hep-ph/9905237] [ɪɴSPIRE].

[52] A.B. Goncharov, *Multiple polylogarithms, cyclotomy and modular complexes*, *Math. Res. Lett.* **5** (1998) 497 [arXiv:1105.2076] [ɪɴSPIRE].

[53] A.B. Goncharov, *Multiple polylogarithms and mixed Tate motives*, math/0103059 [ɪɴSPIRE].

[54] J. Vollinga and S. Weinzierl, *Numerical evaluation of multiple polylogarithms*, *Comput. Phys. Commun.* **167** (2005) 177 [hep-ph/0410259] [ɪɴSPIRE].

[55] Wolfram Research, *Mathematica*, Wolfram Reserach, Champaign, Illinois, U.S.A., 12.1 ed. (2020).

[56] M. Heller and A. von Manteuffel, *MultivariateApart: Generalized partial fractions*, *Comput. Phys. Commun.* **271** (2022) 108174 [arXiv:2101.08283] [ɪɴSPIRE].

[57] W. Decker, G.-M. Greuel, G. Pfister and H. Schönemann, *SINGULAR 4-2-1 — A computer algebra system for polynomial computations*, http://www.singular.uni-kl.de (2021).

[58] B. Agarwal, F. Buccioni, A. von Manteuffel and L. Tancredi, *Two-loop leading colour QCD corrections to $q\bar{q} \to \gamma\gamma g$ and $qg \to \gamma\gamma q$*, *JHEP* **04** (2021) 201 [arXiv:2102.01820] [ɪɴSPIRE].

[59] C. Duhr and F. Dulat, *PolyLogTools — polylogs for the masses*, *JHEP* **08** (2019) 135 [arXiv:1904.07279] [ɪɴSPIRE].

[60] S. Catani, *The Singular behavior of QCD amplitudes at two loop order*, *Phys. Lett. B* **427** (1998) 161 [hep-ph/9802439] [ɪɴSPIRE].

[61] J. Vollinga, *GiNaC: Symbolic computation with C++*, *Nucl. Instrum. Meth. A* **559** (2006) 282 [hep-ph/0510057] [ɪɴSPIRE].

[62] M. Heller, A. von Manteuffel and R.M. Schabinger, *Multiple polylogarithms with algebraic arguments and the two-loop EW-QCD Drell-Yan master integrals*, *Phys. Rev. D* **102** (2020) 016025 [arXiv:1907.00491] [ɪɴSPIRE].